Study on the association of wall shear stress and vessel structural stress with atherosclerosis: an experimental animal study

Zhongzhao Teng PhD[1,2*], Shuo Wang PhD[1], Aziz Tokgoz PhD[2], Valentina Taviani PhD[1], Joseph Bird PhD[3], Umar Sadat MD PhD[4], Yuan Huang PhD[5], Andrew J Patterson PhD[1], Nichola Figg[3], Martin J Graves PhD[1], Jonathan H Gillard MD[1]

1. Department of Radiology, University of Cambridge, Cambridge, United Kingdom
2. Department of Engineering, University of Cambridge, Cambridge, United Kingdom
3. Department of Medicine, University of Cambridge, Cambridge, United Kingdom
4. Cambridge Vascular Unit, Cambridge University Hospitals NHS Foundation Trust, Cambridge, United Kingdom
5. EPSRC Centre for Mathematical and Statistical Analysis of Multimodal Clinical Imaging, University of Cambridge, Cambridge, United Kingdom

Running title: Shear stress, structural stress, atherosclerosis

* Corresponding author

Dr Zhongzhao Teng
Department of Radiology, University of Cambridge
Level 5, Box 218, Addenbrooke's Hospital, Hills Rd.,
Cambridge, CB2 0QQ, UK
Tel: 44 (0)1223 746447
Fax: 44 (0)1223 330915
Email: zt215@cam.ac.uk

Word count: 4, 589

Number of figures and tables: 5

Abstract

Background: Artery is subject to wall shear stress (WSS) and vessel structural stress (VSS) simultaneously. This study is designed to explore the role of VSS in development of atherosclerosis.

Methods: Silastic collars were deployed on the carotid to create two constrictions on 13 rabbits for a distinct mechanical environment at the constriction. MRI was performed to visualise arteries' configuration. Animals with high fat (n=9; Model-group) and normal diet (n=4; Control-group) were sacrificed after 16 weeks. 3D fluid-structure interaction analysis was performed to quantify WSS and VSS simultaneously.

Results: Twenty plaques were found in Model-group and 3 in Control-group. In Model-group, 8 plaques located proximally to the first constriction (Region-1, close to the heart) and 7 distally to the second (Region-2) and 5 plaques were found on the contralateral side of 3 rabbits. Plaques at Region-1 tended to be bigger than those at Region-2 and the macrophage density at these locations was comparable. Minimum time-averaged WSS (TAWSS) in Region-1 was significantly higher than that in Region-2, and both maximum oscillatory shear index (OSI) and particle relative residence time (RRT) were significantly lower. Peak and mean VSS in Region-1 were significantly higher than those in Region-2. Correlation analyses indicated that low TAWSS, high OSI and RRT were only associated with plaque in Region-2, while lesions in Region-1 was only associated with high VSS. Moreover, only VSS was associated with wall thickness of plaque-free regions.

Conclusion: VSS might contribute to the initialisation and development of atherosclerosis solely or in combination with WSS.

Key words: wall shear stress; vessel structural stress; atherosclerosis; artery

Abbreviations

ALE	Arbitrary Lagrangian-Eulerian
CCA	Common carotid artery
CFD	Computational fluid dynamics
EC	Endothelial cell
ECM	Extracellular matrix
FSI	Fluid-structure interaction
HDL	High density lipoprotein
LDL	Low density lipoprotein
Region-1	Proximal to the first constriction (close to the heart)
Region-2	Distal to the second constriction (close to the head)
MR	Magnetic resonance
MTH	Mean thickness of healthy (plaque-free) section
MWT	Maximum wall thickness
OSI	Oscillatory shear index
PAR	Plaque area ratio
PC-MRI	Phase contrast MRI
RRT	Relative resident time
TAWSS	Time averaged wall shear stress
TOF	Time of flight
VH-IVUS	Virtual histology intravascular ultrasound
VSMC	Vascular smooth muscle cell
VSS	Vascular structural stress
WSS	Wall shear stress

1. Introduction

Atherosclerosis is the leading cause of death and disability worldwide[1]. Its development is generally characterised by deposition of extracellular lipids, inward migration of pro-inflammatory cells and proliferation and migration of local vascular smooth muscle cells (VSMCs)[2]. Atherosclerosis is a systemic disease that affects nearly all arterial territories, however, its development rate[3,4] is known to differ locally. Highly advanced lesions are primarily located in areas with bifurcation or a tortuous shape, e.g., arch. This suggests that local environmental factors could influence plaque development.

Arterial wall is subject to two distinct types of mechanical loading due to the dynamic blood pressure and flow. These mechanical loads can be classified into vascular structural stress (VSS) due to arterial expansion induced by dynamic blood pressure and wall shear stress (WSS) acting on the lumen surface due to blood flow. The association between supraphysiological WSS and the malfunctioning of endothelial cells (ECs), and therefore the initialization and development of atherosclerosis has been extensively studied[5], while the role of VSS remains less clear. Regions exposed to low or oscillatory WSS appear to be atherogenic, whereas regions exposed to WSS with high magnitude and uniform direction are protected[6–8]. Slow and oscillatory flow tend to increase the residence time of circulating particles in susceptible regions. Moreover ECs transduce WSS into biochemical signals that regulate gene expression and cell behaviour via specialized mechanisms and pathways, and supraphysiological WSS modifies pathways and contributes to atherosclerosis and vascular malformations[9,10]. However, the general relationship between low and oscillatory WSS and atherosclerosis development failed in several regions of the arterial circulation[11,12], suggesting that other parameters may play an important role in the localization and onset of atherosclerosis.

Under physiological conditions, ECs within the endothelium, as well as the ECs of vasa vasorum are subject to both WSS and VSS simultaneously, while all other cells, including VSMCs, within the wall structure are mainly subject to VSS only. VSS is a complex mechanical stress that acts in circumferential, radial, and axial directions within the wall, causing structural deformation of individual cells. VSMCs are capable of sensing VSS through multiple mechanisms and transducing it into intracellular signals[13,14] that might contribute to the initialization and development of atherosclerosis. The role of VSS in atherogenesis was proposed more than half a century ago based on the fact that atherosclerosis is found in arteries

instead of veins, and is likely to develop at ostia of branches where high VSS concentration occurs[15,16]. This hypothesis was supported by the observation that reduction in arterial intramural stress inhibited atherosclerosis in rabbits[17,18] and vulnerable carotid plaque was found at the location with both low WSS and high local blood pressure as quantified by computational fluid dynamics (CFD) [19]. In case of hypertension, the elevated blood pressure increases VSS and induces compensatory vascular remodelling and subsequently enhances endothelial permeability and vascular tone[20] and superoxide production in VSMC[21]. Ex vivo studies have demonstrated a combination effect of WSS and VSS in modulating EC bioactivities[22,23] and common biochemical pathways in both EC and VSMC have been found to response to both WSS and VSS[24]. Although these observations suggest the potential role of VSS in atherosclerosis initialization, direct evidences are still lacking.

In this study, two constrictions were created on the carotid artery of rabbits by placing a collar to create distinct mechanical environments at different locations that refer to constrictions. In vivo magnetic resonance (MR) imaging was performed to visualize the arteries' configuration and to reconstruct the 3D geometry. Fully coupled fluid-structure interaction (FSI) analyses were performed to calculate WSS and VSS simultaneously. Histopathological stains were used to visualize the plaque distribution and the local inflammatory status. The associations between WSS, VSS and plaque characteristics were reported.

2. Materials and methods

2.1. Rabbit treatment protocol

This study was approved by the local ethics committee and animals were treated according to Home Office animal welfare guidelines. Nine New Zealand White rabbits were put on a high fat diet that comprised of 0.3% cholesterol and 4.7% palm oil in standard rabbit chew for 16 weeks (Model-group) and four rabbits received normal chew diet (Control-group). A non-occlusive, silastic collar (ARK Therapeutics, Finland) was implanted on the left common carotid artery (CCA) of 9 rabbits two weeks after the high fat diet (Fig.1A&B). Collars were also placed in 4 rabbits from the Control-group. Sham operation was performed on the right CCA. The collar had two narrow points constricting to 2 mm external diameter (Fig.1A) and produced a partial occlusion of the artery. Rabbit health status was assessed by serological analysis and body weight. Blood cholesterol, high density lipoprotein (HDL), low density lipoprotein (LDL) and triglyceride levels were measured to monitor the dietary intake of cholesterol and lipids.

2.2. Magnetic resonance imaging

MR imaging was performed three days after collar implantation with bespoke 3D time of flight (TOF), T_1-weighted spin echo, T_2-weighted gradient echo and phase contrast sequences (PC-MRI) to visualise carotid artery structure and measure blood flow velocity (Fig.1B and S_Figure 1 in the **Supplemental Material**). The imaging was performed on a Bruker 4.7T system using a surface coil (Bruker 25-mm coil) with ECG-gating. Detailed scanning parameters for each sequence were, 3D TOF: TR/TE, 16.8/3.5 ms; echo train length (ETL), 1; number of excitations (NEX), 1; Matrix, 256×256; thickness, 0.2930 mm; pixel spacing, 0.2930 mm; T_1-weighted: TR/TE, 700/9 ms; ETL, 1; NEX, 2; Matrix, 512×512; thickness, 2 mm; pixel spacing, 0.125 mm; T_2-weighted: TR/TE, 4458.1/64.7 ms; ETL, 8; NEX, 2; Matrix, 512×512; thickness, 2 mm; pixel spacing, 0.125 mm; PC-MRI: acquisition number, 2; Matrix, 256×256; thickness, 3 mm; pixel spacing, 0.1953 mm; VENC, 150 mm/s.

The silastic collar does not produce any MR signal and the collar therefore appeared hypointense in both T_1-weighted and T_2-weighted images. Following implantation, the void within the collar became filled with interstitial fluid (S_Figure 1 in the **Supplemental Material**) which was hyperintense in both T_1-weighted and T_2-weighted images.

2.3. Mechanical analysis

The lumen, outer wall, collar, and interstitial fluid were identified manually with reviewing TOF, T_1-weighted and T_2-weighted images using VascularView (Tenoke Ltd., Cambridge, UK). The 3D geometry was reconstructed using an in-house developed software in Matlab 2018a (The Mathworks, Inc., MA, USA) and meshed using hexahedral elements in ADINA 9.2.3 (ADINA R&D Inc., MA, USA). Both ends were extended 10 times of the local diameter to eliminate the entrance effects. The detailed structure and fluid domains with mesh were shown in S_Figure 2 in the **Supplemental Material**. Briefly, the arterial cross section was divided into 192×12 subdivisions (~30×10 μm^2) with an axial thickness of 200 μm (S_Figure 2A in the **Supplemental Material**), and the cross section of the fluid domain was divided into 50×50 subdivisions with the same axial thickness as the structure domain (S_Figure 2B in the **Supplemental Material**). A coarser mesh was used for extended sections to reduce the computational cost. The mesh dependency analysis was performed by changing element size with a step of ~10% in each dimension until the difference of the peak VSS and maximum flow

velocity (with 99.5% criterion) were less than 2%[25]. The resulting mesh density was then chosen for the final analysis.

The Young's modulus of silastic collar is 2.05 MPa and the Poisson's ratio is 0.35 as provided by the manufacturer. The arterial wall was assumed to be a hyper-elastic material and characterised by the modified Mooney-Rivlin strain energy density function,

$$W = c_1(\bar{I}_1 - 3) + D_1\left[e^{D_2(\bar{I}_1-3)} - 1\right] + K(J-1) \quad (1)$$

in which $\bar{I}_1 = J^{-2/3}I_1$, I_1 the first invariant of left Cauchy-Green deformation tensor and J is the determinant of deformation gradient; c_1, D_1 and D_2 are empirical material constants and K is the Lagrange multiplier for the incompressibility. Material constants were determined by fitting previously reported experimental data, c_1=1.11 kPa, D_1=3.54 kPa and D_2=0.70[26].

Determination of computational starting shape

Since images were acquired at the pressurised condition with axial stretch[27], shrinkage was necessary to recover the pressure- and stretch-free configuration to generate the starting shape for the computational simulation[28]. Axial shrinkage was set to be 15%, which was determined by the ratio of the length of the arterial section before and after harvesting from the animals in the Control-group. The blood pressure (78-116 mmHg) and waveform were adopted from previous reports[29,30]. Due to the presence of the collar, radial shrinkage rates were different in the region beyond the constrictions, at the constrictions and between the constrictions. The shrinkage for each section was determined such that when pressurised with mean pressure, the configuration matched with the one obtained from in vivo imaging. The radial shrinkage was 10.2±0.7%, 0.1±0.2%, 0.2±0.2% for each of the three sections, respectively.

Fluid-structure interaction analysis

After the shrinkage was determined, the arterial lumen and outer wall contours and the slice thicknesses were updated accordingly, and the 3D geometry was reconstructed (Fig.1B). The interstitial fluid between the artery and collar was modelled as an incompressible gel with material constants set to be c_1=0.0212 kPa, D_1=0.4260 kPa and D_2=0.5312[31]. The volume enclosed by the arterial lumen surface was defined as fluid domain, which was similarly meshed with hexahedral elements.

Blood flow was assumed to be laminar, Newtonian, viscous, and incompressible. Navier-Stokes equations with arbitrary Lagrangian-Eulerian (ALE) formulation were used as the governing equations,

$$\rho_b \frac{\partial \boldsymbol{u}}{\partial t} + \left[\left(\left(\boldsymbol{u} - \boldsymbol{u}_g\right) \cdot \nabla\right)\boldsymbol{u}\right] = -\partial p + \mu \partial^2 \boldsymbol{u}, \quad \nabla \cdot \boldsymbol{u} = 0 \tag{2}$$

with loading conditions,

$$p|_{inlet} = p_{in}(t), \quad p|_{outlet} = p_{out}(t)$$

where $\boldsymbol{u}$ is the flow velocity, $\boldsymbol{u}_g$ is the mesh velocity, p is the pressure, and μ and ρ_b stand for the blood viscosity and density, respectively. The motion of the arterial wall, collar and interstitial fluid was governed by,

$$\rho_w v_{i,tt} = \sigma_{ij,j}, \ i,j=1,2,3; \text{ sum over } j, \tag{3}$$

with boundary condition,

$$\sigma_{ij,j} \cdot n_j\big|_{outter\ wall} = 0$$

in which ρ_w is the wall density, $\boldsymbol{v}$ is the displacement vector, $\boldsymbol{\sigma}$ is the stress tensor, and t denotes time. There was no relative displacement between collar, interstitial fluid, and the arterial outer wall. No-slip condition between the flow-vessel interfaces was set,

$$\boldsymbol{u}|_\Gamma = \frac{\partial \boldsymbol{v}}{\partial t}\bigg|_\Gamma$$

and interaction actions between the fluid and solid was governed by

$$\sigma_{ij}^f \cdot n_j\big|_\Gamma = \sigma_{ij}^s \cdot n_j\big|_\Gamma$$

where Γ represents the inner wall of the vessel and the superscripts, *f* and *s*, stand for fluid part and solid part, respectively. The fully coupled FSI analyses were performed in ADINA 9.2.3. It uses unstructured finite element methods for both fluid and solid models. Nonlinear incremental iterative procedures were used to handle FSI. The governing finite element equations for both solid and fluid models were solved by the Newton-Raphson iteration method. The energy convergence criterion was used for solid domain during equilibrium iterations with the relative energy tolerance being 0.05 and relative force and moment tolerance being 0.01. For the fluid domain, the relative tolerances for velocities, pressure and displacements were set to be 0.06 for controlling the equilibrium. Both the displacement and velocities at the fluid-structure interface and the forces on the structure due to the viscos fluid were checked for convergence. Relative displacement/velocity and force tolerances were both set to be 0.06. Details of the models and methods are given by Bathe[32]. The $p_{out}(t)$ was adjusted such that the difference between the simulated flow rate and the one measured by phase contrast MR

was less than 5%. Each simulation was performed over four cardiac cycles and results from the last one was extracted for analysis.

Mechanical parameters used for analysis

Maximum principal stress was used to characterise VSS. WSS[6,33], oscillatory shear index (OSI)[33] and relative resident time (RRT)[34,35] have been widely suggested to be associated with atherosclerosis initialization and development. OSI was defined as,

$$\mathrm{OSI} = \frac{1}{2}\left(1 - \frac{\left|\int_0^T \vec{\tau} dt\right|}{\int_0^T |\vec{\tau}| dt}\right) \tag{4}$$

in which T is the cardiac period and $\vec{\tau}$ is WSS. RRT at a particular site is inversely proportional to the distance that a particle at that site travels during a cardiac cycle,

$$\mathrm{RRT} \sim \left(\frac{1-2\times\mathrm{OSI}}{T}\int_0^T |\vec{\tau}| dt\right)^{-1} \tag{5}$$

The expression on the right was therefore used as the indicator of RRT to represent the average amount of time that a particle spent in a region. All parameters were extracted using 99.5% criterion to remove any possible distortion due to local poor mesh quality for the final analysis.

VSS is both location and time dependent and can be written VSS (r, θ, z, t) in a cylindrical coordinate system. The peak and mean values of VSS were used to characterise the structural loading in this study,

$$\text{Peak VSS} = \max_t \left\{\max_\Omega [\mathrm{VSS}(r,\theta,z,t)]\right\}, \text{ and Mean VSS} = \frac{1}{\Omega}\frac{1}{T}\int_\Omega \int_0^T \mathrm{VSS}(r,\theta,z,t) dt\, dv \tag{6}$$

in which, Peak VSS is the maximum VSS during one cardiac cycle in a region, Ω, and Mean VSS is the time average value of VSS in a region, and T is the cardiac cycle.

2.4. Immunohistochemical processing and analysis

All 13 rabbits were sacrificed at the end of the 16 weeks. CCAs on both sides were collected (Fig.1C). Collar implants were carefully removed, and constriction points were marked. Standard immunohistochemical procedure was followed. At locations proximal to the first constriction (Region-1; about 6-mm length) and distal to the second constriction (Region-2; about 6-mm length) with a 1-mm gap, 5-μm slices were made for Haematoxylin and Eosin (H&E) and Cluster of Differentiation 68 (CD68) stains. For the arteries obtained on the contralateral side and those from the 4 controlled animals, slices at similar levels were made for H&E and CD68 stains. Each histological slide was digitised using NanoZoomer (Hamamatsu Photonics, Hamamatsu, Japan) at x40 magnification.

An in-house software developed in Matlab was used to perform quantitative histological analysis. Each CD68 image was processed with a semi-automatic Support Vector Machine classifier[36] to segment area with CD68 positive allowing the calculation of area percentage with macrophages. Segmentation parameters of the classifier were optimised with the help of Mrs Nichola Figg, who has more than 15 years of experience in histopathological analysis of diseased arterial tissues. Plaque area ratio (PAR), maximum wall thickness (MWT defined as the maximum thickness in a region) and the mean thickness of healthy (plaque free) section (MTH defined as the mean thickness of all healthy sections in a region) were measured manually in NDP Reviewer (Hamamatsu Photonics, Hamamatsu, Japan) (Fig.2). PAR is defined as the ratio between area in yellow (plaque) and the wall (area in grey + plaque) and MTH is defined as, $(d_1+d_2+d_3+d_4+d_5)/5$. No lipid-rich necrotic core, intraplaque haemorrhage or calcified tissues was found in either Model- or Control-group.

2.5. Statistical analysis

The normality was assessed by examining the quantile-quantile plots. Variables that followed the normal distribution were expressed as mean±standard deviation (Mean±SD), or otherwise median [inter-quantile range, IQR]. Frequencies in categorical data were studied using the Pearson's chi-square test. The difference in plaque characteristics and mechanical variables at different regions on the paired sides were evaluated by Wilcoxon signed rank test. The correlations between plaque characteristics and mechanical variables were assessed using Spearman correlation test and multivariable analyses were further performed to identify the independent factors associated with lesions' features in both regions. The statistical analysis was performed in MATLAB. A significant difference was assumed if $p<0.05$.

3. Results

The final weights of Control (n=4) and Model (n=9) groups were 5.04±0.20 kg and 4.10±0.31 kg, respectively ($p<0.001$). Except for triglycerides, total cholesterol (15.833±5.175 vs. 1.525±0.465, mmol/L, $p<0.001$), LDL (13.100±5.246 vs. 0.525±0.222, mmol/L, $p<0.001$) and HDL (0.962±0.236 vs. 0.665±0.157, mmol/L, $p=0.025$) of Model-group were all significantly higher than those of controls (Table 1). The stenosis, defined by the diameter, caused by the collar at the first constriction point was 30.4%±11.6% and 34.8%±12.2% at the 2nd constriction point ($p=0.324$). The constrictions led to a flow reduction which had not recovered three days

after the collar deployment as quantified by the PC-MRI. The peak and the minimum velocity on the collared side were both significantly lower than those on the contralateral side (72.1±25.1 cm/s vs. 95.1±26.4 cm/s, p<0.0001; 18.9±11.8 cm/s vs. 19.8±14.2 cm/s, p=0.002).

3.1. Location-dependent pathological features

Presence of plaque was defined as the ratio between the plaque (the area in yellow in Fig.2) and the wall area (area in grey + yellow in Fig.2) exceeding 5%. In Model-group, plaques were found in all rabbits with 15 plaques on the collared sides (8 in Region-1 and 7 in Region-2), and five plaques on the contralateral sides (p=0.003). Compared with those on the contralateral side, plaques on the collared side in either Region-1 or Region-2 tended to be bigger and more inflammatory with higher PAR, MWT, MTH and density of macrophages (Fig.3). On the collared side, plaques in Region-1 were bigger than those in Region-2 with a similar level of inflammatory burden (Fig.3).

In Control-group, three plaques (two in Region-1) were found on the collared sides in two animals, and none was observed on the corresponding contralateral sides. In general, Model-group tended to have more plaques than the controls (p=0.045). Although PAR in Model-group was bigger than the one in the control, no significant difference was found (25.4±22.3% vs. 10.5±1.8%, p=0.654), neither as the density of CD68-positive macrophages (median [interquartile range]: 89.2 [34.9, 374.0] vs. 27.7 [13.6, 178.1], p=0.373). However, since the number of plaques in Control-group is small, the test might have rejected the hypothesis incorrectly.

3.2. Location-dependent haemodynamic characteristics

A representative case with haemodynamic parameters on the collared side and corresponding contralateral side was shown in Fig.1E&F. Flow parameters during one cardiac cycle, including time averaged WSS (TAWSS), OSI and RRT were all location dependent (Fig.1E). WSS was significantly highest at the constriction points due to their narrowest dimension and it was lowest in the region right after each constriction. The distribution pattern of OSI and RRT was similar with lowest at the sites of constriction, and highest in the region right after each constriction. The values of WSS, OSI and RRT in Region-1 and in the middle region between the two constrictions were moderate. VSS was shown in Fig.1F. Both of Peak VSS and mean VSS were lowest at the sites of constriction and highest in Region-1 and Region-2.

When the data was pooled, it was found that minimum TAWSS in Region-1 was significantly higher than the one in Region-2 (Fig.4A); both maximum OSI and RRT in Region-1 was significantly lower than the two in Region-2 (Fig.4B&C); and the highest minimum TAWSS, and lowest maximum OSI and RRT appeared on the contralateral side (Fig.4A-C). In the wall structure, arteries without collars had the lowest Peak VSS and Mean VSS. These two parameters reached their highest level in Region-1, while Peak VSS and Mean VSS were moderate in Region-2 (Fig.4D&E).

3.3. The relationship between local mechanical parameters and plaque features

In Region-1, none of flow parameters was associated with PAR, MWT, MTH, or macrophage density. On the contrary, Peak VSS was associated with PAR, MWT and macrophage density with ρ being 0.88 (p=0.003), 0.72 (p=0.037), and 0.70 (p=0.043), respectively. Mean VSS was associated with PAR and macrophage density with ρ being 0.80 (p=0.014) and 0.75 (p=0.025), respectively. In Region-2, both maximum OSI and RRT were associated with PAR significantly with ρ being 0.76 (p=0.040) and 0.81 (p=0.025), respectively. Moreover, both were also associated with the density of macrophage with ρ being 0.85 (p=0.012) and 0.83 (p=0.016), respectively. However, minimum TAWSS did not associate with neither PAR nor macrophage density. Neither Peak VSS nor Mean VSS were associated with any plaque feature in Region-2. When data from Region-1 and Region-2 were pooled, as shown in Fig.2, Peak and Mean VSS, none of flow parameters, correlated positively with local wall thickness either at the location with plaque (Peak VSS: ρ=0.68, p<0.001; Mean VSS: ρ=0.58, p<0.001) or free of plaque (Peak VSS: ρ=0.60, p=0.001; Mean VSS: ρ=0.47, p=0.002).

Spearman correlation analysis showed that Peak and Mean VSS correlated with each other (ρ=0.67, p=0.01), so as maximum OSI and maximum RRT (ρ=0.95, p<0.001). Multivariable regression analyses were therefore performed to further assess the correlation between the three independent haemodynamic factors, Peak VSS, minimum TAWSS, and maximum OSI, and lesions characteristics, including, PAR, MWT, MTH and the density of macrophage. Results indicated that Peak VSS was associated with PAR (slope=0.022, p=0.030), MWT (slope=0.012, p=0.040) and the density of macrophage (slope=2.88, p=0.046) in Region-1; maximum OSI was associated with PAR (slope=0.93, p=0.022), MWT (slope=0.72, p=0.036) and the density of macrophage (slope=1.4×10^3, p=0.0004) in Region-2. More information can be found in the **Supplemental Material** (Tables S1 and S2).

4. Discussion

To authors' best knowledge, this is the first study to quantify the association between local mechanical loadings, including both WSS and VSS simultaneously, and morphological and inflammatory status of atherosclerosis using animal models. Traditional WSS hypothesis could well explain the appearance of plaque in Region-2, however, it failed for those found in Region-1 where TAWSS was higher, and ISO and RRT were lower. Regression analysis demonstrated that high VSS associated well with lesion found in the region proximal to Region-1. This study implied that both WSS and VSS could initialise atherosclerosis solely or in combination.

Previous studies on the biomechanics of atherosclerosis focused largely on the pathological effects of imbalanced flow environment on the vascular physiology[37]. The combined effect of WSS and VSS has been least investigated, although it has been proposed and quantified indirectly previously[19,38]. There is a clear lack of comprehensive studies aimed at understanding the effects of structural stresses and stretches on the pathophysiology of the vessel wall. The preferable appearance of atherosclerotic plaque at the location with bifurcation or bend has been mainly thought to be due to malfunctioned WSS. High VSS might also appear in these locations. As shown in Fig.1 and Fig.4D&E, high VSS concentrations appeared in both Region-1 and Region-2. Only FSI analysis can quantify WSS and VSS simultaneously. However, due to convergence issues arising from irregular wall geometry at these locations, nonlinear material properties, large deformation, and highly nonlinear governing equations, it is challenging to obtain a successful FSI simulation. This might be one of the main reasons that major efforts have been spent on studies seeking the pathological impact of WSS on the atherosclerosis initialization using CFD, while the role of VSS has been ignored. It is worthy to point out that as shown in Fig.4D, although peak VSS in Region-1 was significantly higher than the one in Region-2, the difference in absolute value was small, and mean VSS in these two regions was comparable (Fig.4E). It is due to the small blood pressure difference, 4.46±2.06 mmHg, between these two regions as the collar deployment only induced a mild luminal stenosis in this study. The pressure drop will be apparent when the stenosis is over 50%[39].

The physiological stretch of the vessel wall ranges between 5%-10%. It is beneficial for regulating the normal cellular processes such as angiogenesis[40,41], cell proliferation[42] and extracellular matrix (ECM) remodelling[43]. However high magnitudes of stretches more than 20% are considered pathological[44] that could be induced by increased intramural blood

pressure or irregular local geometry. The artery tends to maintain a certain VSS level by adjusting its thickness[45,46]. As shown in Fig.2, elevated VSS increased the wall thickness locally and VSS correlated very well with local wall thickness either at the location with plaque or free of plaque. The pathological stretch could activate biological pathways. Although hypertension is often associated with excessive levels of WSS, it is also equally responsible for elevated levels of structural stress, particularly at arterial regions with a highly tortuous shape and at bifurcations[47]. Pathophysiological increases in structural loading are known to cause phenotypic adaptations in VSMCs that transform them to dedifferentiated states[14,48,49]. This indicates that, structural loading has the capacity to modulate gene expression, as well as various functions of the VSMCs, such as proliferation, survival and ECM remodelling[8]. Abnormal levels of stretch is known to promote expression of inflammatory genes, such as inducible nitric oxide synthase (iNOS) by macrophages[27,50]. Multivariate regression analyses demonstrated this relationship that peak VSS was associated significantly with the density of CD68 in both Region-1 and Region-2. Pathological stretching is also known to disturb the integrity of ECM by activating macrophage cells to produce MMPs such as MMP-1, MMP-3 and MMP-9[50–52] that are known to weaken fibrous cap mechanical strength. Considering the difference in magnitude (WSS is in the range of 0.001-0.010 kPa and VSS is in the range of 100-1000 kPa) and the strength of fibrous cap (~200 kPa[31]), VSS is thought to be more relevant with atherosclerotic plaque rupture than WSS[53]. Lesions in the region with both low WSS and high local blood pressure tended to be more vulnerable, while those in the region with low WSS only were more stable[19]. Experiments also demonstrated the role of pathological stretch in endothelial dysfunction and cell apoptosis[54]. It is therefore a need to consider the pathological impact of WSS in combination of VSS for a better understanding of atherosclerosis initialization and development.

It is in general believed that in animal models persistently lowered WSS appears to be the principal flow disturbance needed for the formation of higher risk lesions, e.g., thin cap fibroatheroma[55], and larger lesions[37], whereas the regions of increased WSS were protective[37]. However, the role of WSS in the atherosclerosis development might be more complex than we have observed. Results from this study showed that the density of CD68 was associated with minimum TAWSS negatively in Region-2, though, marginally and significantly with maximum OSI. It has been suggested that in human the low WSS in the distal region of the plaque is leading to a stable plaque phenotype, while the regions exposed to high shear stress, e.g., in the proximal site, are softer, and high WSS is, therefore, thought to be associated with

vulnerable plaque features[56]. These were supported to a certain degree by a follow-up study (20 patients) using the combination of virtual histology intravascular ultrasound (VH-IVUS) and CFD[57]. It was observed that compared with intermediate-WSS, low-WSS segments develop greater plaque and necrotic core progression, and high-WSS segments develop greater necrotic core and calcium progression, regression of fibrous and fibrofatty tissue, and excessive expansive remodelling, suggestive of transformation to a more vulnerable phenotype. Furthermore, a very recent 12-month follow-up study (40 patients) using the combination of VH-IVUS, CFD and structure-only analysis shown a complex interplay of WSS and VSS in the change of plaque size and composition[38]. Areas with high VSS are associated with compositional changes consistent with increased plaque vulnerability and areas with low WSS are associated with more plaque growth in areas that progress and less plaque loss in areas that regress. These results emphasize the need to consider WSS and VSS in an integrative way for the understanding the atherosclerosis.

In addition to WSS, OSI and RRT, other WSS-derived parameters, such as WSS gradient (WSSG)[58] and wall shear stress angle gradient (WSSAG)[59], were proposed to be associated with atherosclerosis initialisation and development. However, as summarised in the review[7] that the evidence for the low/oscillatory shear theory is less robust than commonly assumed. Further studies and analyses are needed for a better understanding on the mechanisms of atherosclerotic diseases. Moreover, as shown in this study and others[38], WSS and VSS might work in combination to initiate atherosclerosis and promote its development. Matrices combining both structure and fluid parameters, e.g., VSS/WSS, VSS×OSI, VSS×RRT, etc., could better characterise atherosclerotic diseases. However, the physiological and pathological backgrounds of these combined matrices are unclear and required further exploration.

Despite of interesting findings, limitations exist: (1) artery wall was assumed as an isotropic material; (2) the residual stress in the wall was not considered as it is not measurable using any current non-invasive approach; (3) the blood pressure of each animal was not measured, that is, the loading condition was not animal-specific; (4) extracellular fluid flow within the structure induced by solid deformation was not considered. However, such a flow should be extremely slow due to the tiny extracellular space; (5) the deployment of collar modulated mechanical environment acting on the endothelium and within the wall structure in both regions and it is therefore impossible to evaluated the pathological impact of WSS and VSS

individually; (6) the deployment of collar did not mimic the stenosis induced by the presence of carotid atherosclerotic plaque, but created distinct mechanical environments at different regions to explore the association between WSS and VSS and atherosclerosis initialization; (7) further studies should be performed to explore the combined effect of other aspects, such as the density and biofunction of VSMC; (8) haemodynamic parameters and plaque histopathologic features as well as their relationship were characterised in region based and the extract location matched analysis was not performed; and (9) the flow velocity might change over time after the collar deployment. However, in this study PC-MRI was only performed once three days after the deployment. The evaluation of effect of flow velocity change on the VSS and WSS was, therefore, not possible.

Author contributions

ZT designed the study, performed data analysis and drafted the manuscript; SW and AZ performed data analysis and revised the manuscript; VT, AJP and MJG developed MR sequences and performed the imaging; JB built the animal model and performed the histology stain; US and JHG revised the manuscript significantly; and NF analysed the histology.

Acknowledgement

This study was supported by ARTreat FP7 European Research Council, Engineering and Physical Sciences Research Council (EPSRC) (EP/P021654/1), British Heart Foundation (BHF) (PG/11/74/29100 and PG/18/14/33562) and National Institute for Health Research (NIHR) Cambridge Biomedical Research Centre. Dr Wang was supported by China Scholarship Council and Dr Tokgoz by an EPSRC Doctoral Training Award at the University of Cambridge.

Disclosure

Dr Teng is the Chief Scientist of Tenoke Ltd., UK and Nanjing Jingsan Medical Science & Technology Ltd., China. Other authors do not have any conflict of interests to disclose.

References

1. Mendis S PP and NB. Global Atlas on Cardiovascular Disease Prevention and Control. *Geneva World Heal Organ*. 2011.
2. Libby P, Ridker PM, Hansson GK. Progress and challenges in translating the biology of atherosclerosis. *Nature*. 2011;473(7347):317-325. doi:10.1038/nature10146
3. Cheruvu PK, Finn A V, Gardner C, et al. Frequency and distribution of thin-cap fibroatheroma and ruptured plaques in human coronary arteries: a pathologic study. *J Am Coll Cardiol*. 2007;50(10):940-949. doi:10.1016/j.jacc.2007.04.086
4. Wykrzykowska JJ, Mintz GS, Garcia-Garcia HM, et al. Longitudinal distribution of plaque burden and necrotic core-rich plaques in nonculprit lesions of patients presenting with acute coronary syndromes. *JACC Cardiovasc Imaging*. 2012;5(3 Suppl):S10-8. doi:10.1016/j.jcmg.2012.01.006
5. Pedrigi RM, Mehta V V, Bovens SM, et al. Influence of shear stress magnitude and direction on atherosclerotic plaque composition. *R Soc Open Sci*. 2016;3(10):160588. doi:10.1098/rsos.160588
6. Caro CG, Fitz-Gerald JM, Schroter RC. Arterial wall shear and distribution of early atheroma in man. *Nature*. 1969;223(5211):1159-1160. doi:10.1038/2231159a0
7. Peiffer V, Sherwin SJ, Weinberg PD. Does low and oscillatory wall shear stress correlate spatially with early atherosclerosis? A systematic review. *Cardiovasc Res*. 2013;99(2):242-250. doi:10.1093/cvr/cvt044
8. Kwak BR, Bäck M, Bochaton-Piallat ML, et al. Biomechanical factors in atherosclerosis: mechanisms and clinical implications. *Eur Hear J*. 2014;35(43):3013-3020, 3020a-3020d. doi:10.1093/eurheartj/ehu353
9. Baeyens N, Bandyopadhyay C, Coon BG, Yun S, Schwartz MA. Endothelial fluid shear stress sensing in vascular health and disease. *J Clin Invest*. 2016;126(3):821-828. doi:10.1172/jci83083
10. Baratchi S, Khoshmanesh K, Woodman OL, Potocnik S, Peter K, McIntyre P. Molecular Sensors of Blood Flow in Endothelial Cells. *Trends Mol Med*. 2017;23(9):850-868. doi:10.1016/j.molmed.2017.07.007
11. Joshi AK, Leask RL, Myers JG, Ojha M, Butany J, Ethier CR. Intimal thickness is not associated with wall shear stress patterns in the human right coronary artery. *Arter Thromb Vasc Biol*. 2004;24(12):2408-2413. doi:10.1161/01.ATV.0000147118.97474.4b
12. van der Giessen AG, Schaap M, Gijsen FJ, et al. 3D fusion of intravascular ultrasound

and coronary computed tomography for in-vivo wall shear stress analysis: a feasibility study. *Int J Cardiovasc Imaging*. 2010;26(7):781-796. doi:10.1007/s10554-009-9546-y

13. Qiu J, Zheng Y, Hu J, et al. Biomechanical regulation of vascular smooth muscle cell functions: from in vitro to in vivo understanding. *J R Soc Interface*. 2014;11(90):20130852. doi:10.1098/rsif.2013.0852
14. Haga JH, Li YS, Chien S. Molecular basis of the effects of mechanical stretch on vascular smooth muscle cells. *J Biomech*. 2007;40(5):947-960. doi:10.1016/j.jbiomech.2006.04.011
15. Niimi H. Role of stress concentration in arterial walls in atherogenesis. *Biorheology*. 1979;16(3):223-230. doi:10.3233/bir-1979-16311
16. De Langen CD. The pressure gradient in the arterial wall and the problem of arteriosclerosis. *Cardiologia*. 1953;22(5):315-319. doi:10.1159/000165293
17. Thubrikar MJ, Baker JW, Nolan SP. Inhibition of atherosclerosis associated with reduction of arterial intramural stress in rabbits. *Arteriosclerosis*. 1988;8(4):410-420. doi:10.1161/01.atv.8.4.410
18. Tropea BI, Schwarzacher SP, Chang A, et al. Reduction of aortic wall motion inhibits hypertension-mediated experimental atherosclerosis. *Arter Thromb Vasc Biol*. 2000;20(9):2127-2133. doi:10.1161/01.atv.20.9.2127
19. Chen YC, Bui AV, Diesch J, et al. A novel mouse model of atherosclerotic plaque instability for drug testing and mechanistic/therapeutic discoveries using gene and microRNA expression profiling. *Circ Res*. 2013. doi:10.1161/CIRCRESAHA.113.301562
20. Birukova AA, Chatchavalvanich S, Rios A, Kawkitinarong K, Garcia JG, Birukov KG. Differential regulation of pulmonary endothelial monolayer integrity by varying degrees of cyclic stretch. *Am J Pathol*. 2006;168(5):1749-1761. doi:10.2353/ajpath.2006.050431
21. Inoue N, Kawashima S, Hirata KI, et al. Stretch force on vascular smooth muscle cells enhances oxidation of LDL via superoxide production. *Am J Physiol*. 1998;274(6):H1928-32. doi:10.1152/ajpheart.1998.274.6.H1928
22. Amaya R, Pierides A, Tarbell JM. The Interaction between Fluid Wall Shear Stress and Solid Circumferential Strain Affects Endothelial Gene Expression. *PLoS One*. 2015;10(7):e0129952. doi:10.1371/journal.pone.0129952
23. Dancu MB, Berardi DE, Vanden Heuvel JP, Tarbell JM. Asynchronous shear stress

and circumferential strain reduces endothelial NO synthase and cyclooxygenase-2 but induces endothelin-1 gene expression in endothelial cells. *Arter Thromb Vasc Biol*. 2004;24(11):2088-2094. doi:10.1161/01.ATV.0000143855.85343.0e

24. Lu D, Kassab GS. Role of shear stress and stretch in vascular mechanobiology. *J R Soc Interface*. 2011;8(63):1379-1385. doi:10.1098/rsif.2011.0177
25. Tang D, Yang C, Kobayashi S, et al. 3D MRI-based anisotropic FSI models with cyclic bending for human coronary atherosclerotic plaque mechanical analysis. *J Biomech Eng*. 2009;131(6):061010. doi:10.1115/1.3127253
26. Williams C, Liao J, Joyce EM, et al. Altered structural and mechanical properties in decellularized rabbit carotid arteries. *Acta Biomater*. 2009;5(4):993-1005. doi:10.1016/j.actbio.2008.11.028
27. Bergel DH. The static elastic properties of the arterial wall. *J Physiol*. 1961;156(3):445-457. doi:10.1113/jphysiol.1961.sp006686
28. Huang Y, Teng Z, Sadat U, et al. Non-uniform shrinkage for obtaining computational start shape for in-vivo MRI-based plaque vulnerability assessment. *J Biomech*. 2011;44(12):2316-2319. doi:10.1016/j.jbiomech.2011.06.014
29. O'Rourke MF. From theory into practice: arterial haemodynamics in clinical hypertension. *J Hypertens*. 2002;20(10):1901-1915. doi:10.1097/00004872-200210000-00002
30. Kurashina T, Sakamaki T, Yagi A, Nakamura T, Sakamoto H, Nushiro N. A new device for indirect blood pressure measurement in rabbits. *Jpn Circ J*. 1994;58(4):264-268. doi:10.1253/jcj.58.264
31. Teng Z, Feng J, Zhang Y, et al. A uni-extension study on the ultimate material strength and extreme extensibility of atherosclerotic tissue in human carotid plaques. *J Biomech*. 2015;48(14):3859-3867. doi:10.1016/j.jbiomech.2015.09.037
32. KJ. B. Finite Element Procedures. . *New Jersey Prentice Hall*. 1996.
33. Kawaguchi T, Nishimura S, Kanamori M, et al. Distinctive flow pattern of wall shear stress and oscillatory shear index: similarity and dissimilarity in ruptured and unruptured cerebral aneurysm blebs. *J Neurosurg*. 2012;117(4):774-780. doi:10.3171/2012.7.Jns111991
34. Sugiyama S, Niizuma K, Nakayama T, et al. Relative residence time prolongation in intracranial aneurysms: a possible association with atherosclerosis. *Neurosurgery*. 2013;73(5):767-776. doi:10.1227/neu.0000000000000096
35. Himburg HA, Grzybowski DM, Hazel AL, LaMack JA, Li XM, Friedman MH. Spatial

comparison between wall shear stress measures and porcine arterial endothelial permeability. *Am J Physiol Hear Circ Physiol*. 2004;286(5):H1916-22. doi:10.1152/ajpheart.00897.2003

36. J. CN and S-T. *An Introduction to Support Vector Machines and Other Kernel-Based Learning Methods.* Cambridge, UK: Cambridge University Press; 2000.
37. Cheng C, Tempel D, van Haperen R, et al. Atherosclerotic lesion size and vulnerability are determined by patterns of fluid shear stress. *Circulation*. 2006;113(23):2744-2753. doi:10.1161/circulationaha.105.590018
38. Costopoulos C, Timmins LH, Huang Y, et al. Impact of combined plaque structural stress and wall shear stress on coronary plaque progression, regression, and changes in composition. *Eur Heart J*. 2019;40(18):1411-1422. doi:10.1093/eurheartj/ehz132
39. Chen Z, Qin H, Liu J, et al. Characteristics of Wall Shear Stress and Pressure of Intracranial Atherosclerosis Analyzed by a Computational Fluid Dynamics Model: A Pilot Study. *Front Neurol*. 2020. doi:10.3389/fneur.2019.01372
40. Zheng W, Christensen LP, Tomanek RJ. Differential effects of cyclic and static stretch on coronary microvascular endothelial cell receptors and vasculogenic/angiogenic responses. *Am J Physiol Hear Circ Physiol*. 2008;295(2):H794-800. doi:10.1152/ajpheart.00343.2008
41. Zheng W, Christensen LP, Tomanek RJ. Stretch induces upregulation of key tyrosine kinase receptors in microvascular endothelial cells. *Am J Physiol Hear Circ Physiol*. 2004;287(6):H2739-45. doi:10.1152/ajpheart.00410.2004
42. Li W, Sumpio BE. Strain-induced vascular endothelial cell proliferation requires PI3K-dependent mTOR-4E-BP1 signal pathway. *Am J Physiol Hear Circ Physiol*. 2005;288(4):H1591-7. doi:10.1152/ajpheart.00382.2004
43. von Offenberg Sweeney N, Cummins PM, Birney YA, Cullen JP, Redmond EM, Cahill PA. Cyclic strain-mediated regulation of endothelial matrix metalloproteinase-2 expression and activity. *Cardiovasc Res*. 2004;63(4):625-634. doi:10.1016/j.cardiores.2004.05.008
44. Jufri NF, Mohamedali A, Avolio A, Baker MS. Mechanical stretch: physiological and pathological implications for human vascular endothelial cells. *Vasc Cell*. 2015;7:8. doi:10.1186/s13221-015-0033-z
45. Owens CD. Adaptive changes in autogenous vein grafts for arterial reconstruction: clinical implications. *J Vasc Surg*. 2010;51(3):736-746. doi:10.1016/j.jvs.2009.07.102
46. Ren L, Shi M, Wu Y, et al. Correlation between hypertension and common carotid

artery intima-media thickness in rural China: a population-based study. *J Hum Hypertens*. 2018;32(8-9):548-554. doi:10.1038/s41371-018-0074-x

47. Reed D, Reed C, Stemmermann G, Hayashi T. Are aortic aneurysms caused by atherosclerosis? *Circulation*. 1992;85(1):205-211. doi:10.1161/01.cir.85.1.205
48. Chaabane C, Otsuka F, Virmani R, Bochaton-Piallat ML. Biological responses in stented arteries. *Cardiovasc Res*. 2013;99(2):353-363. doi:10.1093/cvr/cvt115
49. Shyu KG. Cellular and molecular effects of mechanical stretch on vascular cells and cardiac myocytes. *Clin Sci*. 2009;116(5):377-389. doi:10.1042/cs20080163
50. McWhorter FY, Davis CT, Liu WF. Physical and mechanical regulation of macrophage phenotype and function. *Cell Mol Life Sci*. 2015;72(7):1303-1316. doi:10.1007/s00018-014-1796-8
51. Pugin J, Dunn I, Jolliet P, et al. Activation of human macrophages by mechanical ventilation in vitro. *Am J Physiol*. 1998;275(6):L1040-50. doi:10.1152/ajplung.1998.275.6.L1040
52. Wehner S, Buchholz BM, Schuchtrup S, et al. Mechanical strain and TLR4 synergistically induce cell-specific inflammatory gene expression in intestinal smooth muscle cells and peritoneal macrophages. *Am J Physiol Gastrointest Liver Physiol*. 2010;299(5):G1187-97. doi:10.1152/ajpgi.00452.2009
53. Sadat U, Teng Z, Gillard JH. Biomechanical structural stresses of atherosclerotic plaques. *Expert Rev Cardiovasc Ther*. 2010;8(10):1469-1481. doi:10.1586/erc.10.130
54. Kou B, Zhang J, Singer DR. Effects of cyclic strain on endothelial cell apoptosis and tubulogenesis are dependent on ROS production via NAD(P)H subunit p22phox. *Microvasc Res*. 2009;77(2):125-133. doi:10.1016/j.mvr.2008.08.001
55. Pedrigi RM, Poulsen CB, Mehta V V, et al. Inducing Persistent Flow Disturbances Accelerates Atherogenesis and Promotes Thin Cap Fibroatheroma Development in D374Y-PCSK9 Hypercholesterolemic Minipigs. *Circulation*. 2015;132(11):1003-1012. doi:10.1161/circulationaha.115.016270
56. Gijsen F, van der Giessen A, van der Steen A, Wentzel J. Shear stress and advanced atherosclerosis in human coronary arteries. *J Biomech*. 2013;46(2):240-247. doi:10.1016/j.jbiomech.2012.11.006
57. Samady H, Eshtehardi P, McDaniel MC, et al. Coronary artery wall shear stress is associated with progression and transformation of atherosclerotic plaque and arterial remodeling in patients with coronary artery disease. *Circulation*. 2011;124(7):779-788. doi:10.1161/circulationaha.111.021824

58. Tardy Y, Resnick N, Nagel T, Gimbrone MA, Dewey CF. Shear stress gradients remodel endothelial monolayers in vitro via a cell proliferation-migration-loss cycle. *Arterioscler Thromb Vasc Biol*. 1997. doi:10.1161/01.ATV.17.11.3102

59. Augst AD, Ariff B, Thom SAGMG, Xu XY, Hughes AD. Analysis of complex flow and the relationship between blood pressure, wall shear stress, and intima-media thickness in the human carotid artery. *Am J Physiol - Hear Circ Physiol*. 2007. doi:10.1152/ajpheart.00989.2006

Tables and Figures

Table 1. Final weight and cholesterol level at the end of 16-week high fat diet

	Control (n=4)	Modelled (n=9)	p-value
Weight (kg)	5.04±0.20	4.10±0.31	<0.001
Total cholesterol (mmol/L)	1.525±0.465	15.833±5.175	<0.001
LDL (mmol/L)	0.525±0.222	13.100±5.246	<0.001
HDL (mmol/L)	0.665±0.157	0.962±0.236	0.025
Triglycerides (mmol/L)	0.675±0.310	1.656±1.654	0.121
Maximum wall thickness (mm)	0.12 [0.12, 0.13]	0.15 [0.12, 0.23]	0.373
Mean healthy wall thickness (mm)	0.07 [0.07, 0.07]	0.07 [0.07, 0.09]	1.0

Figure 1. Reconstructed 3D geometry based on baseline MR images, images of arteries removed from the animals and corresponding CD68 stain for the visualization of tissue inflammation and calculated flow parameters and mechanical loading within the structure (A: schematic drawing showing the collar geometry and dimension; B: MR-based 3D geometry reconstruction; C: artery with collar and the corresponding contralateral removed from an animal; D: CD68 stain showing macrophages in brown; E: calculated time averaged WSS, OSI and RRT; F: Peak VSS and Mean VSS along the artery wall thickness)

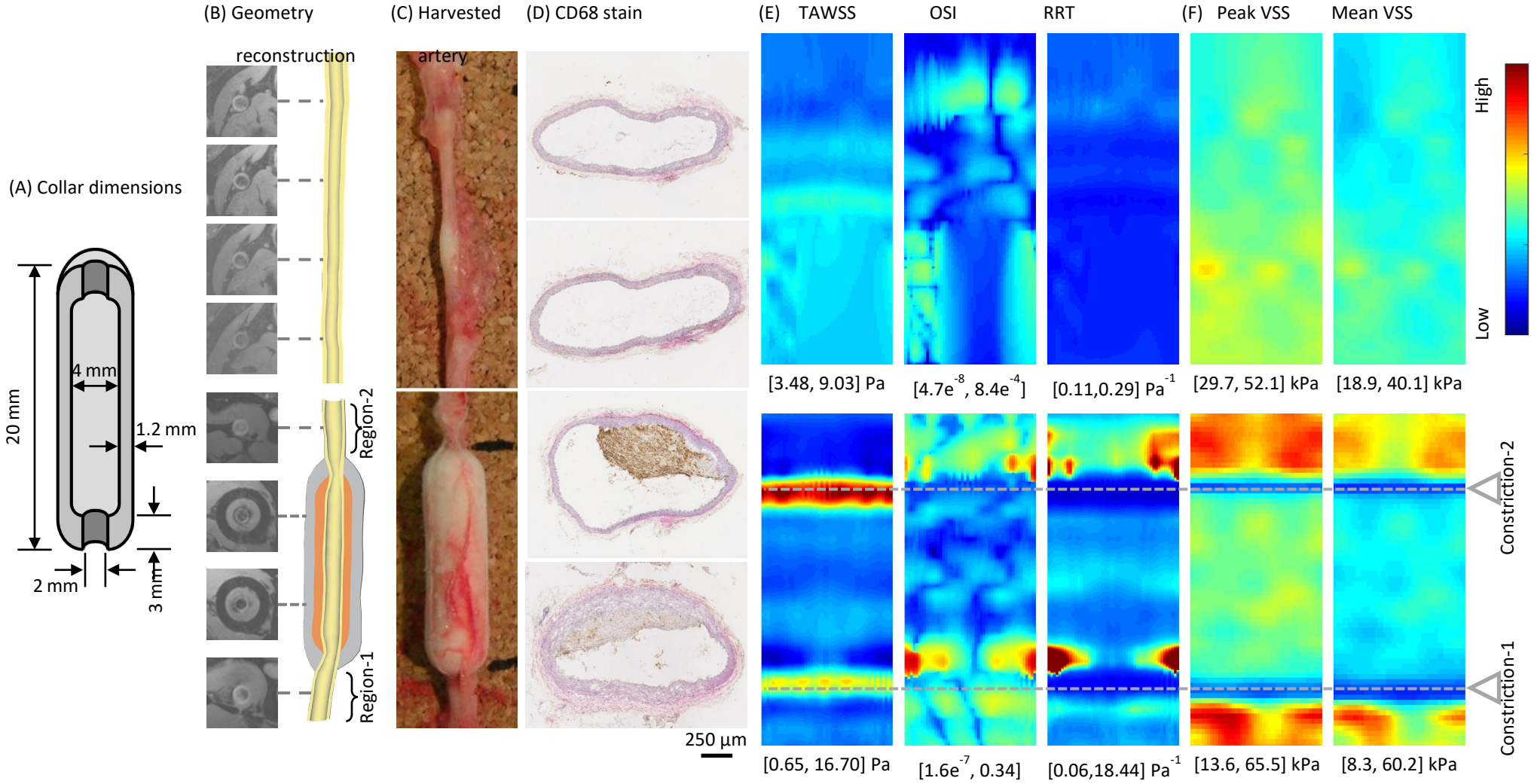

Figure 2. A representative image showing wall and plaque segmentation (left) and the relationship between wall thickness and local vessel structural stress (peak and mean structural stresses; right) (area marked in yellow showing the region with plaque and the one in grey is wall; MWT is the maximum wall thickness and mean wall thickness of the healthy section, MTH=(d_1+d_2+d_3+d_4+d_5)/5).

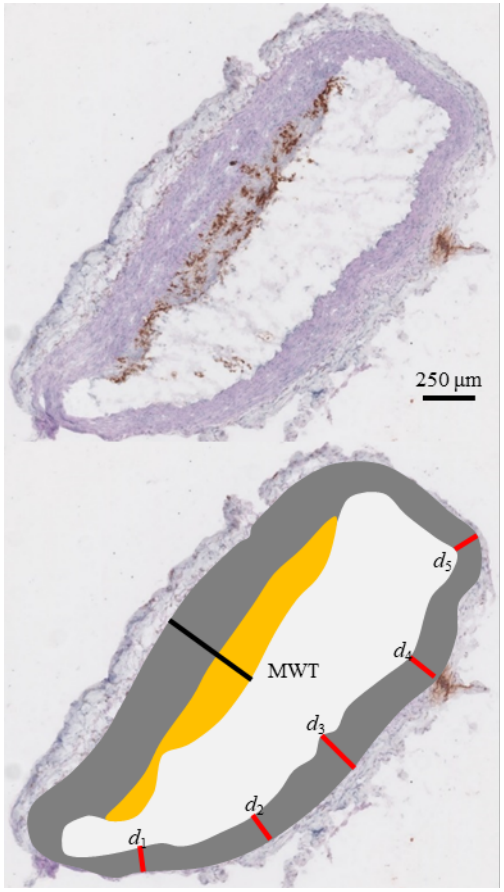

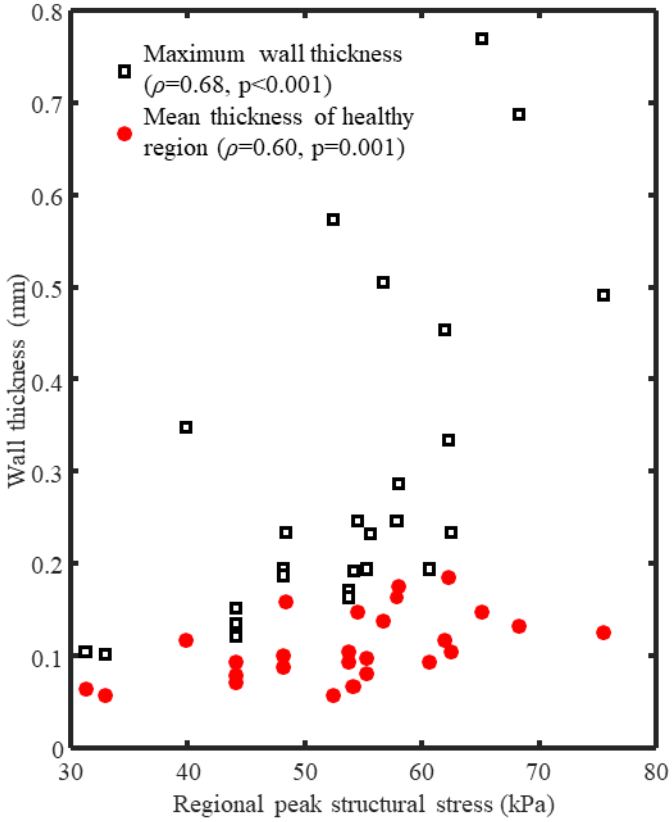

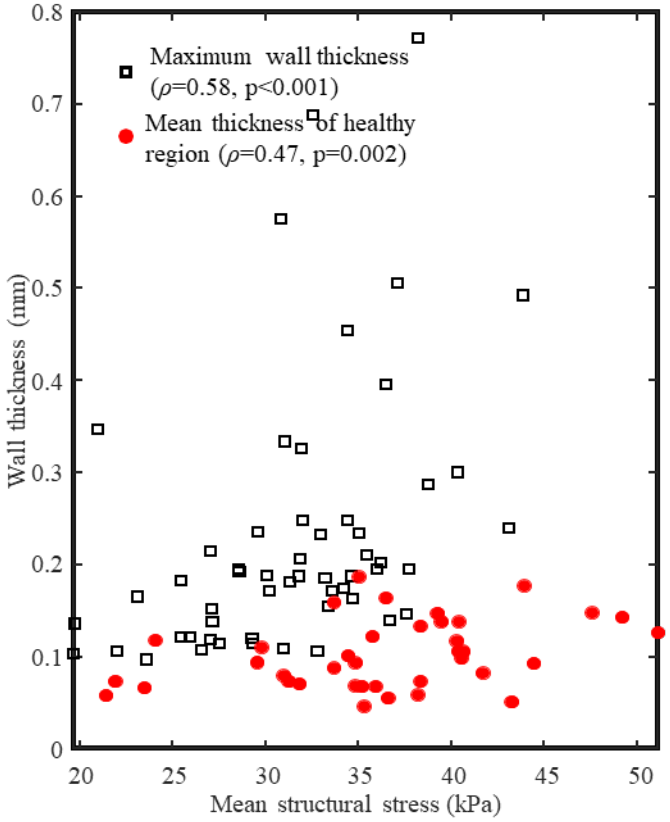

Figure 3. The comparison of plaque morphological and inflammatory features at different location (A: Plaque area ratio (PAR); B: Maximum wall thickness (MWT); C: Mean wall thickness of the healthy section (MTH); and D: The density of CD68-positive macrophage)

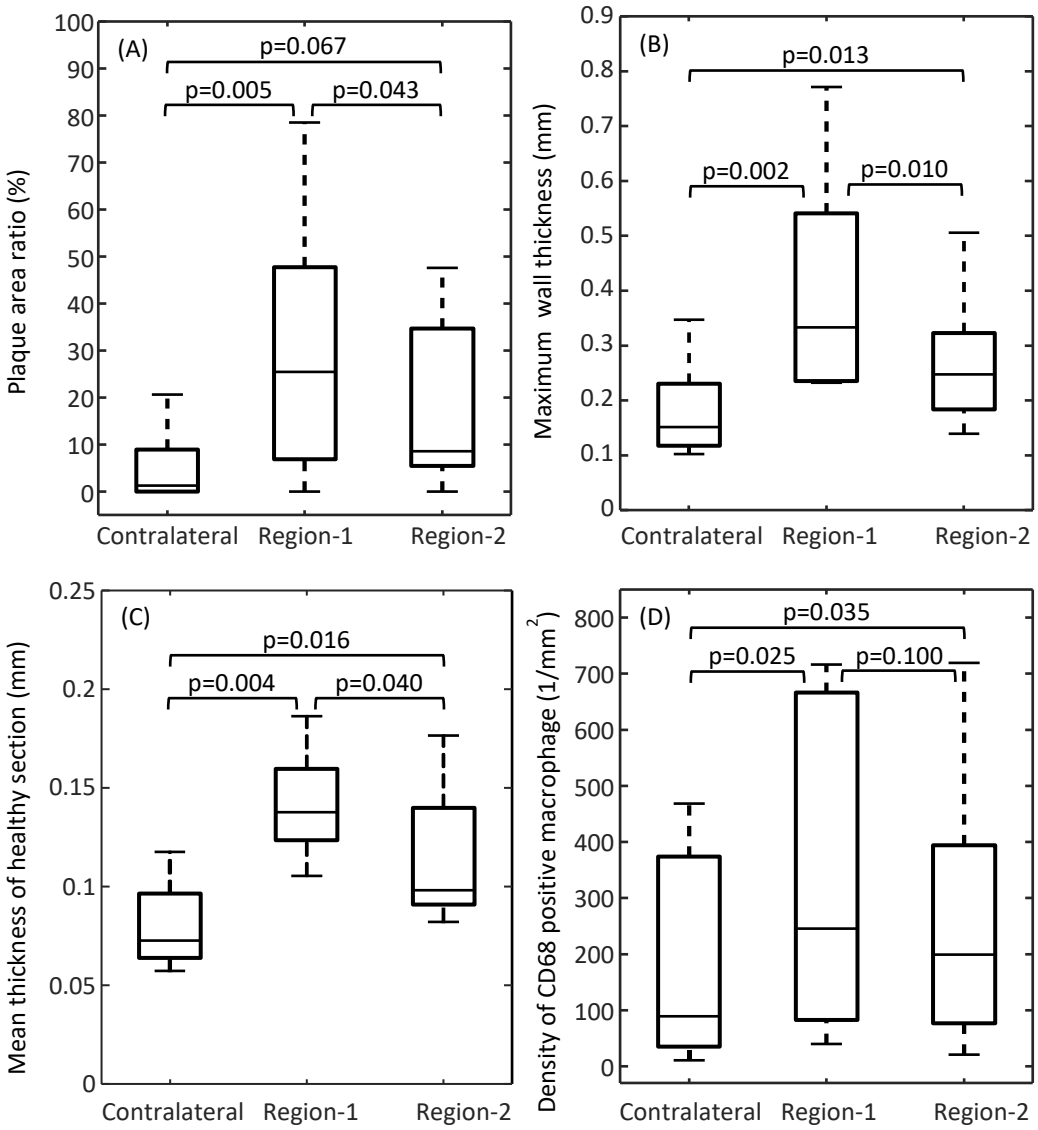

Figure 4. The comparison of mechanical parameters at different location (A: Minimum time averaged wall shear stress (TAWSS); B: Maximum oscillatory shear index (OSI); C: Maximum relative residence time (RRT); D: Peak vessel structural stress (VSS) during one cardiac cycle; E: Mean VSS)

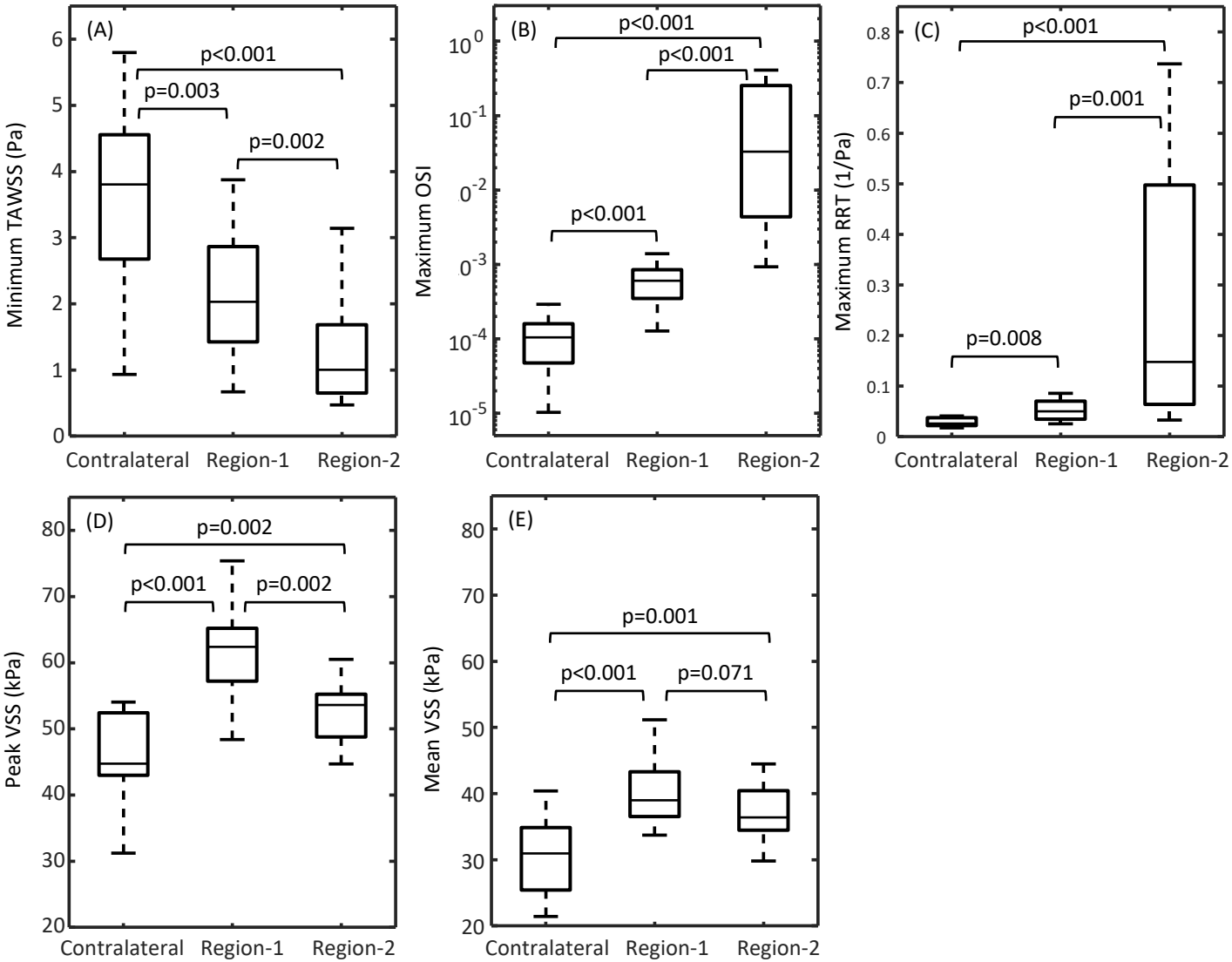

Supplemental Material

to Z Teng, et al., Study on the association of wall shear stress and vessel structural stress with atherosclerosis: an experimental animal study

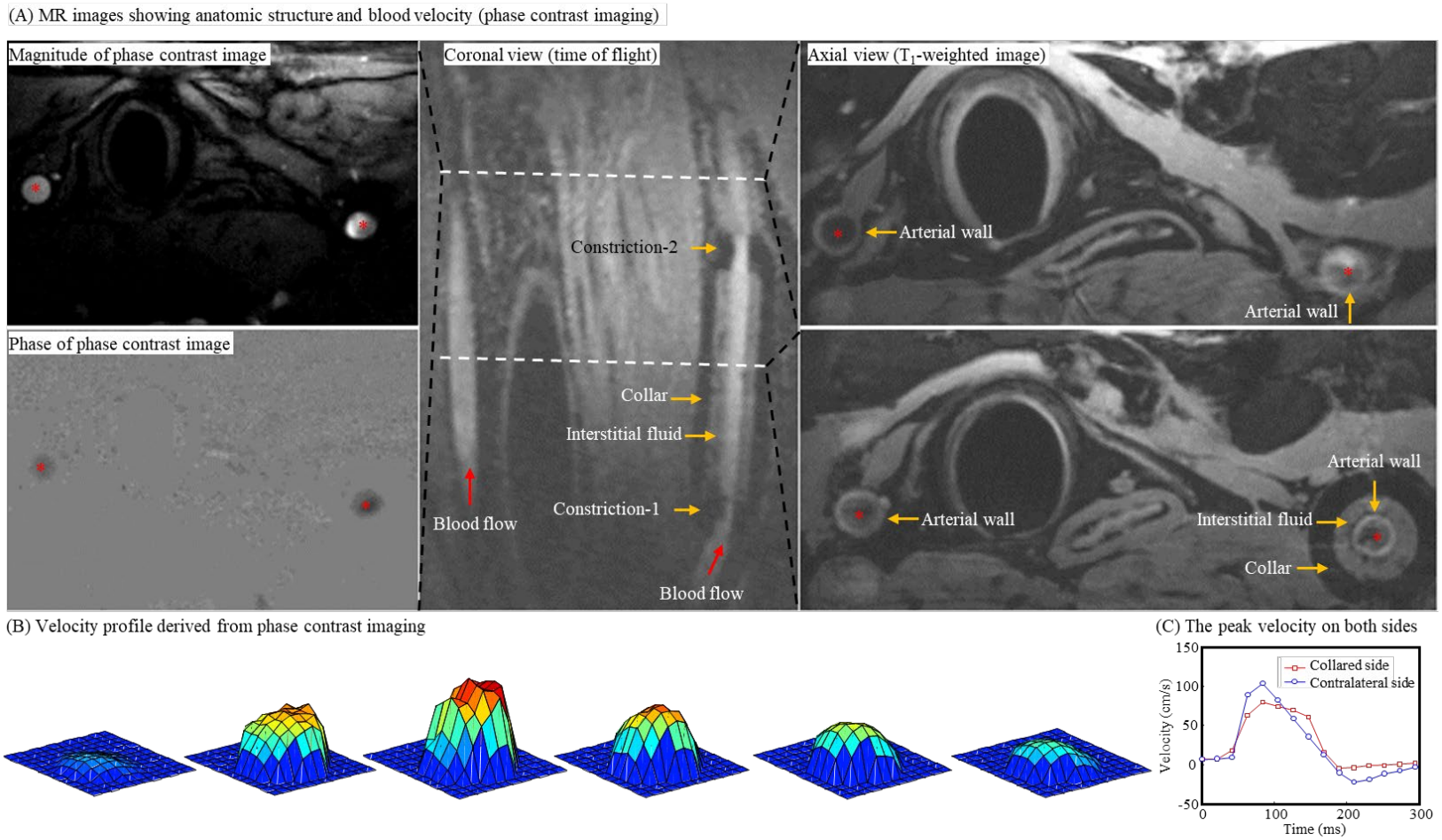

S_Figure 1. In vivo magnetic resonance imaging showing rabbit carotid arteries with and without collar and corresponding blood flow velocity measurements (A: MR images showing the anatomic structure in different view plane and blood velocity [the 1st column is magnitude and phase images from phase contrast imaging; the 2nd column is the time of flight image in the coronal view; the last column is the T_1-weighted images in the axial view at different locations]; B: the blood flow velocity profile derived from phase contrast imaging on the collared side with a 20-ms interval between each frame (the peak velocity was 111.4 cm/s for this case); C: the peak blood flow velocity during one cardiac cycle on collared and contralateral sides)

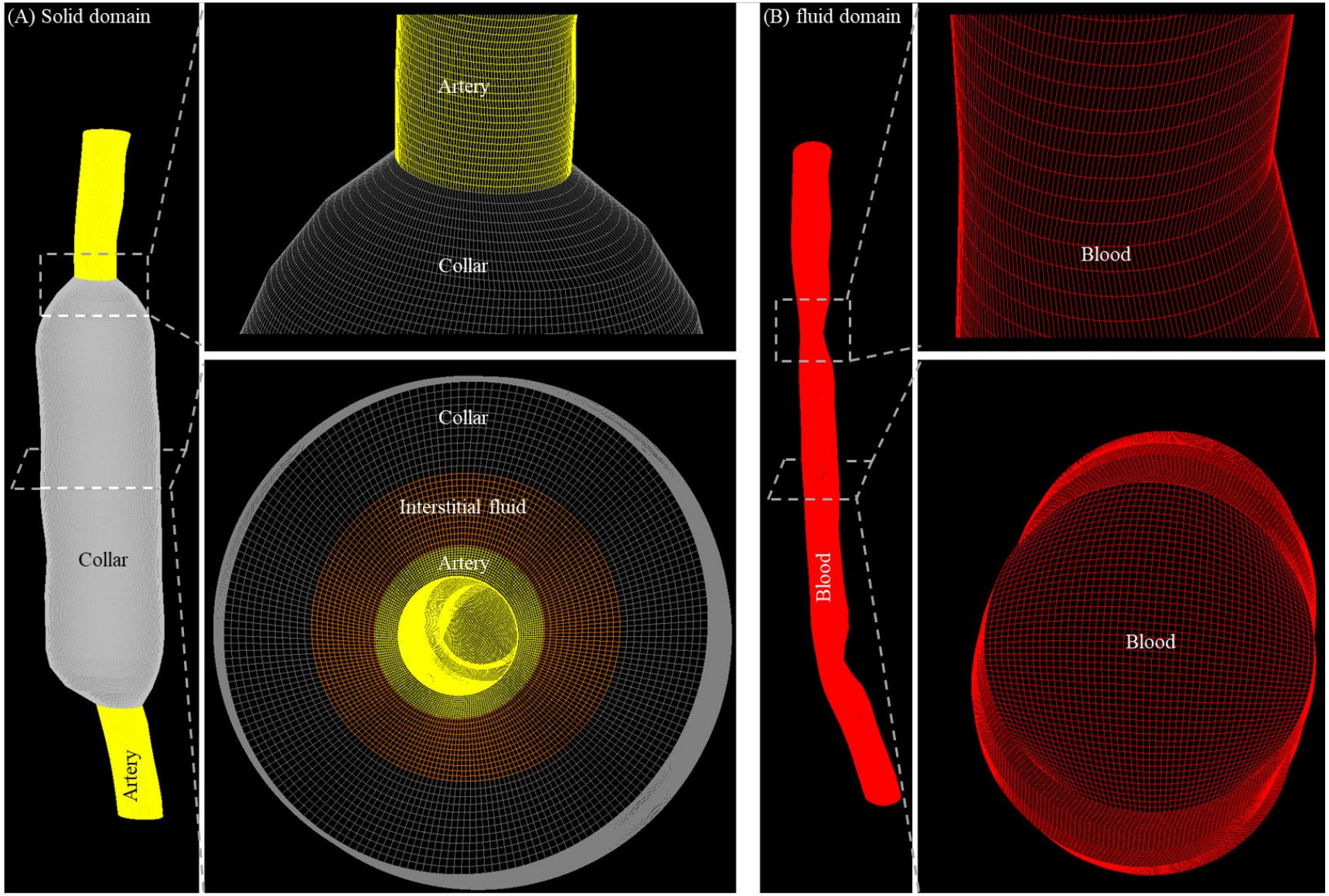

S_Figure 2. Representative images showing structural meshes of solid (A) and fluid (B) domains

Location-specific multivariate analysis confirmed the significant correlations between VSS, wall thickness, PAR and macrophage density in Region-1 (Table S1) and the significant correlations between Max OSI and PAR, MWT and macrophage density in Region-2 (Table S2), after adjusting for other parameters.

Table S1. Multivariate linear regression in Region-1.

	Intercept	Peak VSS	Minimum TAWSS	Maximum OSI
PAR	-0.91, p=0.15	**0.022, p=0.030**	-0.0066, p=0.240	120.95, p=0.570
MWT	-0.15, p=0.79	**0.012, p=0.040**	-0.0099, p=0.290	153.36, p=0.520
MTH	206, p=0.06	0.0012, p=0.390	-0.00055, p=0.700	27.80, p=0.470
CD68	-1143, p=0.18	**2.88, p=0.046**	0.81, p=0.950	5.2×10^{4}, p=0.870

Table S2. Multivariate linear regression in Region-2.

	Intercept	Peak VSS	Minimum TAWSS	Maximum OSI
PAR	-0.75, p=0.19	0.014, p=0.190	-0.0027, p=0.870	**0.93, p=0.022**
MWT	-0.54, p=0.23	0.012, p=0.180	0.0040, p=0.780	**0.72, p=0.036**
MTH	-0.038, p=0.84	0.0021, p=0.430	0.0045, p=0.510	0.03, p=0.780
CD68	-1162.1, p=0.01	**26, p=0.045**	-31.36, p=0.057	**1.4×10^{3}, p=0.0004**